

## Discovery of Novel PPAR Ligands by a Virtual Screening Approach Based on Pharmacophore Modeling, 3D Shape, and Electrostatic Similarity Screening

Patrick Markt,<sup>†</sup> Rasmus K. Petersen,<sup>‡</sup> Esben N. Flindt,<sup>‡</sup> Karsten Kristiansen,<sup>§</sup> Johannes Kirchmair,<sup>||</sup> Gudrun Spitzer,<sup>⊥</sup> Simona Distinto,<sup>†</sup> Daniela Schuster,<sup>†,||</sup> Gerhard Wolber,<sup>||</sup> Christian Laggner,<sup>†</sup> and Thierry Langer<sup>\*,†,||</sup>

Department of Pharmaceutical Chemistry, Institute of Pharmacy and Center for Molecular Biosciences Innsbruck (CMBI), University of Innsbruck, Innrain 52c, 6020 Innsbruck, Austria, BioLigands, International Science Park, Odense, Denmark, Department of Biochemistry and Molecular Biology, University of Southern Denmark, Campusvej 55, 5230 Odense M, Denmark, Inte:Ligand Softwareentwicklungs- and Consulting GmbH, Clemens Maria Hofbauer-Gasse 6, 2344 Maria Enzersdorf, Austria, Department of Theoretical Chemistry, Institute of General, Inorganic, and Theoretical Chemistry, University of Innsbruck, Innrain 52a, 6020 Innsbruck, Austria

Received February 6, 2008

Peroxisome proliferator-activated receptors (PPARs) are important targets for drugs used in the treatment of atherosclerosis, dyslipidaemia, obesity, type 2 diabetes, and other diseases caused by abnormal regulation of the glucose and lipid metabolism. We applied a virtual screening workflow based on a combination of pharmacophore modeling with 3D shape and electrostatic similarity screening techniques to discover novel scaffolds for PPAR ligands. From the resulting 10 virtual screening hits, five tested positive in human PPAR ligand-binding domain (hPPAR-LBD) transactivation assays and showed affinities for PPAR in a competitive binding assay. Compounds **5**, **7**, and **8** were identified as PPAR- $\alpha$  agonists, whereas compounds **2** and **9** showed agonistic activity for hPPAR- $\gamma$ . Moreover, compound **9** was identified as a PPAR- $\delta$  antagonist. These results demonstrate that our virtual screening protocol is able to enrich novel scaffolds for PPAR ligands that could be useful for drug development in the area of atherosclerosis, dyslipidaemia, and type 2 diabetes.

### Introduction

PPARs are fatty acid activated transcription factors which belong to the nuclear receptor family. The  $\alpha$ ,  $\delta$ , and  $\gamma$  subtypes of PPAR coordinate pathways involved in glucose and lipid homeostasis.<sup>1</sup> PPAR- $\alpha$  is expressed at high levels in organs with high capacity of fatty acid oxidation such as the liver, brown adipose tissue, heart, kidney, and intestine. Agonists of this PPAR subtype decrease serum triglyceride levels, increase circulating high-density lipoproteins (HDL), and improve glucose tolerance. Furthermore, the activation of PPAR- $\alpha$  decreases monocyte activation and thereby causes the regression of atherosclerotic lesions. Moreover, PPAR- $\alpha$  activation reduces weight gain by either increasing fatty acid metabolism or energy expenditure.<sup>2,3</sup> Fibrates represent PPAR- $\alpha$  agonists that are currently used in the therapy of dyslipidemia. Antagonists of the PPAR- $\alpha$  subtype are examined for their ability to inhibit the replication of hepatitis C virus.<sup>4a</sup>

Compared to PPAR- $\alpha$ , PPAR- $\delta$  can be found in a more broad range of tissues. Activation of this PPAR subtype has beneficial effects on glucose and lipid metabolism by decreasing fasting insulin and increasing serum HDL levels. In addition, PPAR- $\delta$  activation improves atherosclerosis and reduces diet-induced obesity by enhancing fatty acid oxidation and energy expenditure. Evidence suggests that agonists of the delta subtype are useful in the treatment of type 2 diabetes and diet-induced obesity.<sup>2</sup> Because elevated expression of PPAR- $\delta$  has been observed in cancer cells, antagonists of PPAR- $\delta$  are investigated for their use in anticancer therapy.<sup>5–7</sup>

Expressed in adipose tissue, PPAR- $\gamma$  increases insulin sensitivity and exerts antiatherogenic effects. Glitazones are U.S. Food and Drug Administration (FDA) approved antidiabetes drugs that operate by activating PPAR- $\gamma$ .<sup>2</sup> A side effect of glitazones is weight gain, which is caused by increasing adipocyte differentiation and fatty acid storage. On that account, partial agonists of PPAR- $\gamma$  with decreased side effects on adipose tissue are investigated for their usability in the therapy of type 2 diabetes.<sup>8</sup> Beyond, there is evidence to suggest that PPAR- $\gamma$  antagonists can be used not only as antiobesity drugs but also as antidiabetic drugs.<sup>9</sup>

**PPAR Activation.** To regulate gene expression, PPARs heterodimerize with the retinoid x receptor (RXR). PPAR-RXR target genes can be activated by ligands of either RXR or PPARs.<sup>10</sup> PPAR agonists induce transcription by recruiting coactivator proteins, whereas in the absence of PPAR activators, the recruitment of corepressor complexes represses gene expression.<sup>2</sup>

The Y-shaped ligand-binding pocket of PPAR is large and therefore binds a multitude of fatty acids and synthetic ligands. PPAR- $\alpha$  possesses the largest and most hydrophobic pocket for ligands among the three subtypes. PPAR- $\gamma$  has a more polar and smaller pocket than PPAR- $\alpha$ , followed by a substantially smaller PPAR- $\delta$  pocket. The PPAR pockets can be divided into three arms. Arm I consists of mainly polar residues and includes

\* To whom correspondence should be addressed. Present address: Prestwick Chemical Inc., 67400 Strasbourg-Illkirch. Phone: +33-369-201-616. E-mail: thierry.langer@prestwickchemical.fr.

<sup>†</sup> Department of Pharmaceutical Chemistry, Institute of Pharmacy and Center for Molecular Biosciences Innsbruck (CMBI), University of Innsbruck.

<sup>‡</sup> BioLigands.

<sup>§</sup> Department of Biochemistry and Molecular Biology, University of Southern Denmark.

<sup>||</sup> Inte:Ligand Softwareentwicklungs- and Consulting GmbH.

<sup>⊥</sup> Department of Theoretical Chemistry, Institute of General, Inorganic, and Theoretical Chemistry, University of Innsbruck.

<sup>a</sup> Abbreviations: AF-2 helix, activation function helix 2; AUC, area under the ROC curve; AUC25, normalized area under the ROC curve up to a false positive rate of 25%; DMEM, Dulbeccos modified Eagle's media; CS, calf serum; ECFP, extended connectivity fingerprints; ET\_combo, electrostatic Tanimoto combo score; ET\_pb, Poisson–Boltzmann electrostatic Tanimoto coefficient; FDA, U.S. Food and Drug Administration; HDL, high-density lipoprotein; hPPAR-LBD, human PPAR ligand-binding domain; MEF, mouse embryo fibroblast; PDB, Brookhaven Protein Data Bank; PPAR, peroxisome proliferator-activated receptor; ROC, receiver operating characteristic; RXR, retinoid x receptor; SSP, similarity search protocol; ST, shape Tanimoto.

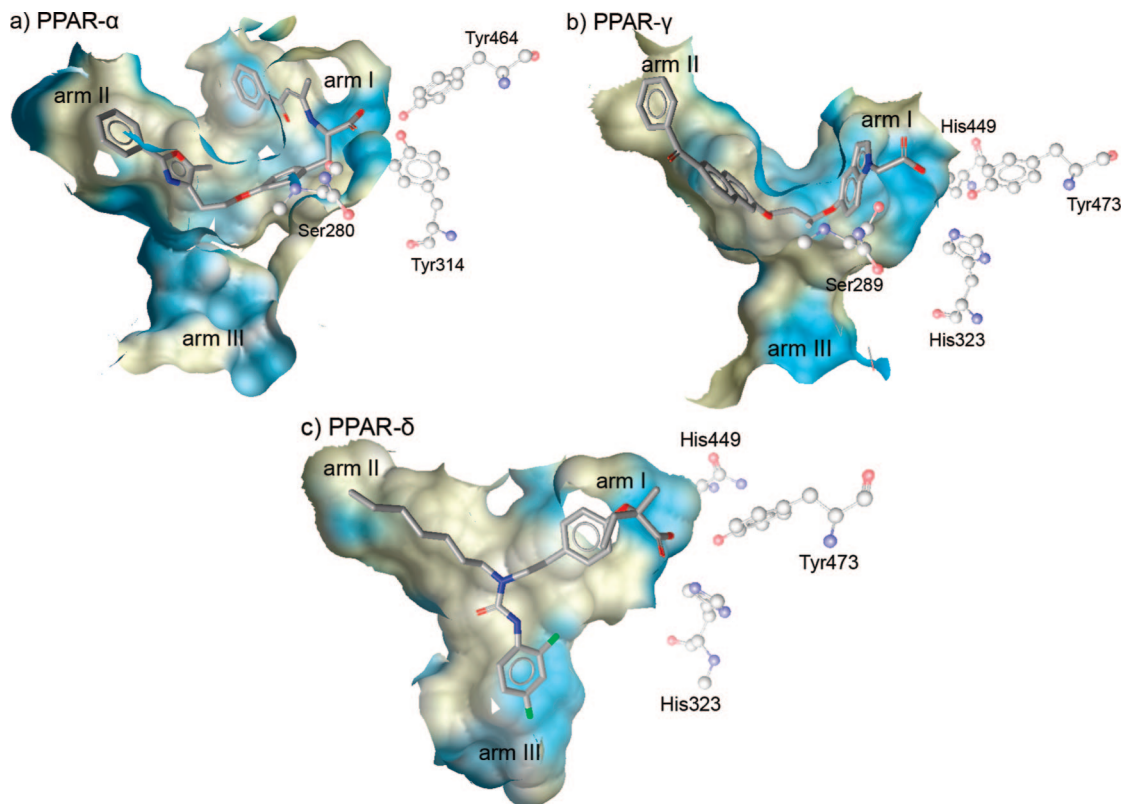


**Figure 1.** PPAR- $\alpha$  (a), PPAR- $\gamma$  (b), and PPAR- $\delta$  (c) ligand-binding pocket colored by lipophilicity. The ligand-binding pockets from the PDB entries 1k7l (PPAR- $\alpha$  complexed with GW409544), 2f4b (PPAR- $\gamma$  complexed with the ligand with the CAS number 853652-40-1), and 1y0s (PPAR- $\delta$  complexed with GW2331) were visualized using the software LigandScout. Hydrophobic areas are shown in yellow, whereas polar parts of the ligand-binding pocket are colored in blue. Active site residues involved in the formation of the hydrogen bond network are displayed as ball and stick models.

the activation function helix 2 (AF-2 helix), which activates transcription if the hydrophilic headgroup of the PPAR agonist (e.g., a carboxylic acid moiety or a thiazolidinedione group) forms a hydrogen bond network with the corresponding residues of the helix. This network stabilizes a conformation of the AF-2 helix that allows the binding of coactivator proteins, which in turn leads to gene transcription. PPAR- $\alpha$  residues involved in the formation of this hydrogen bond network with the ligand are Tyr464, Tyr314, and Ser280 (Figure 1a). In contrast to that, in the PPAR- $\gamma$  (Figure 1b) and PPAR- $\delta$  (Figure 1c) protein hydrogen bonds between the ligand and residues Tyr473, His449, His323, and Ser289 stabilize the active conformation of the AF-2-helix.

The hydrophobic moiety of PPAR agonists either interacts with the hydrophobic arm II (tail up pocket) or with the partly hydrophilic arm III (entrance region of the ligand-binding pocket, tail down pocket). Some PPAR agonists with a branched hydrophobic moiety are able to interact with both hydrophobic arms. Among the ligand-binding pockets of the three PPAR subtypes, the shape of arm III but not of arm I and arm II is conserved. Therefore, the subtype specificity of PPAR agonists depends on the shape of these two arms. Especially, the shape of arm I of PPAR- $\delta$  is narrower in the area next to the AF-2-helix than the corresponding arm of the PPAR- $\alpha$  and PPAR- $\gamma$  pocket.<sup>1,11–14</sup>

Antagonists of PPAR often contain a larger substituted amide group instead of the hydrophilic group. The larger appendix of the headgroup displaces the AF2-helix-stabilizing residues from their position in the ligand-binding domain of the activated PPAR, destroys the charge clamp, and thereby allows the recruitment of corepressor proteins that suppress gene transcription.<sup>15,16</sup>

Because the three PPAR subtypes regulate pathways involved in glucose and lipid metabolism, ligands of all PPAR subtypes represent promising tools for pharmacological research or potential drugs for treating diseases such as atherosclerosis, diet-induced obesity, dyslipidaemia, and type 2 diabetes. Taking this into consideration, we applied a combination of pharmacophore modeling methods with 3D shape and electrostatic similarity search techniques in order to screen commercial compound libraries for new PPAR- $\alpha$ , PPAR- $\delta$ , and PPAR- $\gamma$  agonist scaffolds. The biological evaluation of the selected compounds resulted not only in novel PPAR- $\alpha$  and PPAR- $\gamma$  agonists but also in a compound that exerts both PPAR- $\gamma$  agonistic and PPAR- $\delta$  antagonistic activity. To our knowledge, a similar approach has not been reported yet in the field of PPAR drug discovery.

## Results

**Virtual Screening Using Pharmacophore Models.** At the beginning of our virtual screening workflow, pharmacophore modeling, a fast and well proven virtual screening technique, was applied. The software LigandScout<sup>17</sup> was used to derive structure-based pharmacophore models from crystallographic data of agonist–PPAR complexes found in the Brookhaven Protein Data Bank (PDB).<sup>18</sup> Moreover, ligand-based models were created by subjecting compound sets comprising structurally diverse PPAR agonists to the HipHop algorithm<sup>19</sup> implemented in the Catalyst software package.<sup>20</sup> The discriminatory power of the resulting pharmacophore models was estimated by screening a test set comprising 357 PPAR ligands and a virtual database including 12775 PPAR decoys (see Experimental Section). The validation results were expressed as

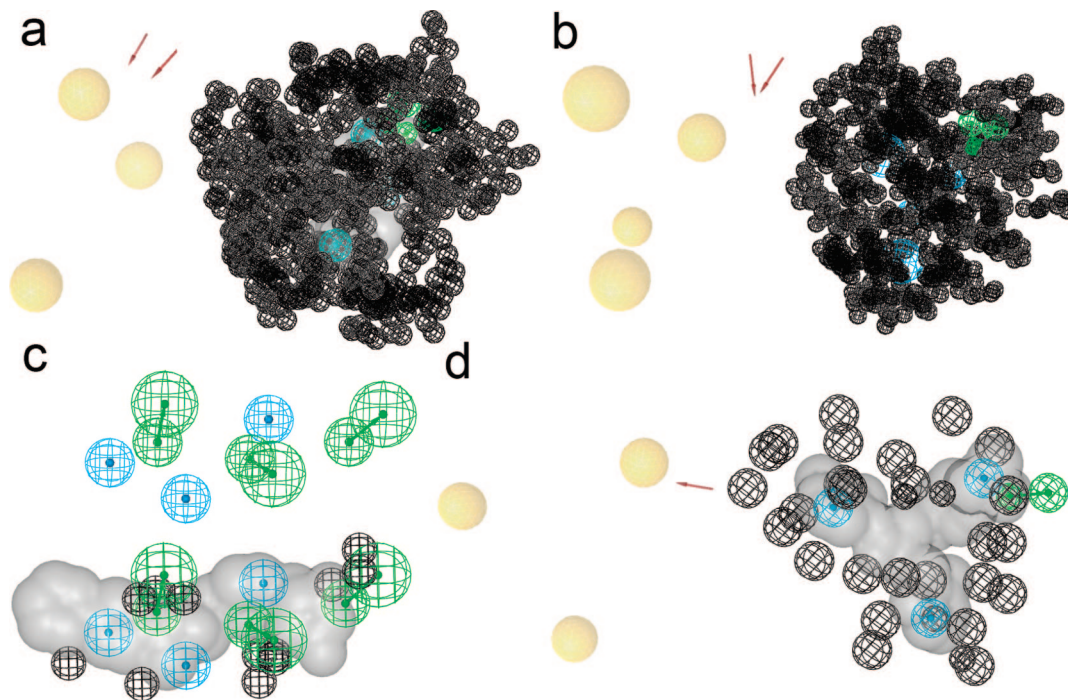


**Figure 2.** Overview of the complexity of *PPAR- $\alpha$  agonist model 1* (a), *PPAR- $\alpha$  agonist model 2* (b), *PPAR- $\gamma$  agonist model* (c), and *PPAR- $\delta$  agonist model* (d). Structure-based models were generated within LigandScout and refined within Catalyst, whereas ligand-based models were created using the HipHop algorithm of Catalyst. LigandScout displays hydrogen bond acceptors as red arrows and hydrophobic interactions as yellow spheres. In Catalyst, green vectors represent hydrogen bond acceptors, blue spheres show hydrophobic interactions, black spheres display excluded volume spheres, which are areas a compound is not allowed to map, and gray clouds represent Catalyst shape.

enrichment factors. The most selective pharmacophore model for PPAR- $\alpha$  agonists, which was named *PPAR- $\alpha$  agonist model 1*, represented a structure-based model derived from the PDB agonist-PPAR- $\alpha$  complex 1k7l (Figure 2a).

On the basis of the crystallographic data of the PDB agonist-PPAR- $\delta$  complex 1y0s, *PPAR- $\alpha$  agonist model 2* was initially categorized as a pharmacophore model for PPAR- $\delta$  agonists until a virtual screen of the test set and the virtual database revealed that it matches more PPAR- $\alpha$  agonists than activators of the  $\delta$ -subtype (Figure 2b). Consequently, a higher enrichment factor for PPAR- $\alpha$  agonists was calculated and the model was categorized as an unselective PPAR- $\alpha$  agonist model. The ligand-based *PPAR- $\gamma$  agonist model*, the best model for PPAR- $\gamma$  agonists, was generated by using a compound set including 14 PPAR- $\gamma$  agonists found in literature as input for the HipHop algorithm (Figure 2c). Finally, the most selective pharmacophore model for PPAR- $\delta$  agonists, *PPAR- $\delta$  agonist model*, was based on the ligand-protein interactions retrieved from the PDB agonist-PPAR- $\delta$  complex 1gwx (Figure 2d). The generation and validation process of these four pharmacophore models is described in the Experimental Section and in more detail in ref 21.

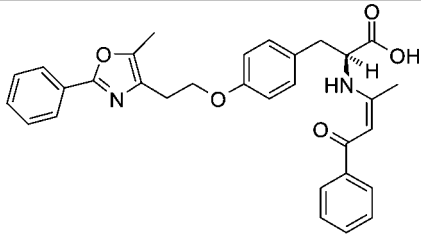
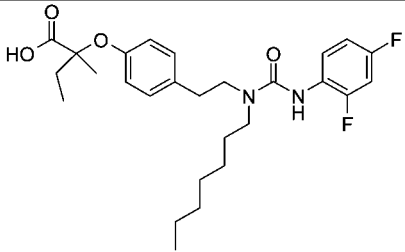
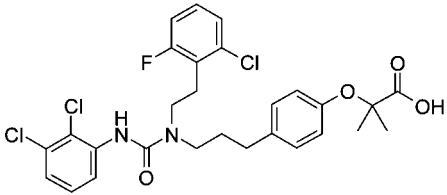
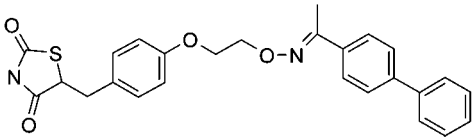
Seven commercial libraries comprising a total of 1063848 compounds were screened within Catalyst. Afterward, Catalyst Fast Fit values were calculated in order to rank the retrieved compounds. Each PPAR agonist model was used to screen all seven commercial libraries. From each resulting hit list, only the best 1000 compounds with respect to their Fast Fit values were kept. Therefore, 28 hit lists, including the top-ranked 1000 compounds, were produced. Because not every PPAR agonist model was able to match 1000 compounds in each commercial library and because duplicate structures resulting from overlapping virtual screening hit lists were deleted by a Pipeline Pilot script, the pharmacophore modeling part of our study resulted in 14311 virtual screening hits.

**Physicochemical Property Filtering of Virtual Screening Hits.** A Pipeline Pilot script was executed to filter the 14311 virtual screening hits obtained from the pharmacophore modeling approach with respect to their physicochemical properties (see Experimental Section). The filter criteria were derived from the physicochemical properties of the 321 PPAR agonists of the PPAR ligand test set, which is described in ref 21. Therefore, only virtual screening hits with physicochemical properties similar to known PPAR agonists were kept. There were 5898 virtual screening hits that matched these filter criteria. These hits formed the so-called focused compound library, which was subjected to 3D shape and electrostatic similarity screening.

**3D Shape and Electrostatic Similarity Screening of a Focused Compound Library.** Because both 3D shape and electrostatic potential are important for the biological activity of compounds and the combination of 3D shape and electrostatic similarity screening has been reported to be a valuable virtual screening tool for the discovery of novel ligand scaffolds, this virtual screening technique was applied to rescore the prefiltered focused compound library.<sup>22,23</sup> To compare the 3D shape and electrostatic potentials between known PPAR agonists and structures of the focused compound library, four similarity search protocols (SSPs), including four different query molecules, were generated and validated. The PPAR agonists GW409544, GW2331, and GW2433 included in the three PDB entries used for the generation of *PPAR- $\alpha$  agonist model 1* (1k7l), *PPAR- $\alpha$  agonist model 2* (1y0s), and *PPAR- $\delta$  agonist model* (1gwx) served as query molecules for SSP 1, 2, and 3, respectively (Table 1).

The PPAR agonist with the CAS number 264908-19-2 from which the Catalyst shape of the ligand-based *PPAR- $\gamma$  agonist model* was derived was used as query molecule for SSP4 (Table 1). The discriminatory power of these four SSPs was validated by screening the 321 PPAR agonists of the PPAR ligand test

**Table 1.** Structures of the PPAR Agonists Utilized as Query Molecules for 3D Shape and Electrostatic Similarity Screening<sup>a</sup>

SSP	PDB entry	ref.	PPAR agonist	structure
1	1k7l	11	GW409544	
2	1y0s	51	GW2331	
3	1gwx	1	GW2433	
4	-	52	264908-19-2 <sup>#</sup>	

<sup>a</sup> # = CAS number of the compound.

set and the 12775 decoys of the virtual database, which both had been applied for the evaluation of the PPAR agonist models.<sup>21,24</sup> The validation results for the four SSPs were analyzed using the receiver operating characteristic (ROC) curve method.<sup>25</sup> The area under the ROC curve metric (AUC) was used to determine the best SSP. For SSP1, an AUC value of 0.797 was calculated, which means that in eight out of ten cases, a randomly selected PPAR agonist is ranked higher by SSP1 than a randomly selected virtual database molecule. ROC curve analysis of SSP2 resulted in an AUC value of 0.952. A nearly identical AUC value of 0.953 was retrieved for SSP3. Finally, an AUC value of 0.956 was calculated for SSP4 (Figure 3).

Only compounds ranked at the top of a hit list ordered by the default EON score ET\_combo will be selected for biological testing. Thus, a SSP which has a high AUC value but ranks many PPAR agonists at the end of the rank-ordered list will be less useful than a SSP with a significantly lower AUC value which assigns more of the highest ranks to PPAR agonists. Because the three SSPs with AUC values above 0.9 (SSP 2, 3, and 4) retrieved about 95% of all active molecules within the top-ranked 25% of the validation compound set, we decided to select our candidates for biological testing from the highest scored 25% of the focused compound library. Therefore, for each SSP, the area under the ROC up to the top-ranked 25% of

the validation compound set was measured and divided by 0.25 to get an easily manageable metric limited between 0 and 1, which is called AUC25.<sup>26</sup> An AUC25 value of 0.512 was calculated for SSP 1, whereas for SSP 2, 3, and 4, a value of 0.852, 0.860, and 0.856 was obtained, respectively. SSP 1 was discarded because of these results and because of its significant lower AUC value for the ROC curve above all thresholds compared to SSP 2, 3, and 4. However, the validation results for the other three SSPs were nearly identical. Therefore, all three SSPs were used to virtually screen the focused compound library for PPAR agonists. The resulting three hit lists were ranked according to the ET\_combo score. The highest ranked 25% of each hit list was kept. Duplicate virtual screening hits were deleted using a Pipeline Pilot script.

**Structural Similarity Analysis of Virtual Screening Hits.** The virtual screening hits obtained by 3D shape and electrostatic similarity screening were subjected to a structural diversity analysis, which was performed by executing a Pipeline Pilot script that calculates Tanimoto similarities between structural fingerprints (see Experimental Section). Then 147 clusters were retrieved when a maximum allowed Tanimoto dissimilarity of 0.7 was used. The clustered compounds were investigated visually for chemical stability. For example, compounds that could be cleaved in aqueous solution because of hydrolyzable

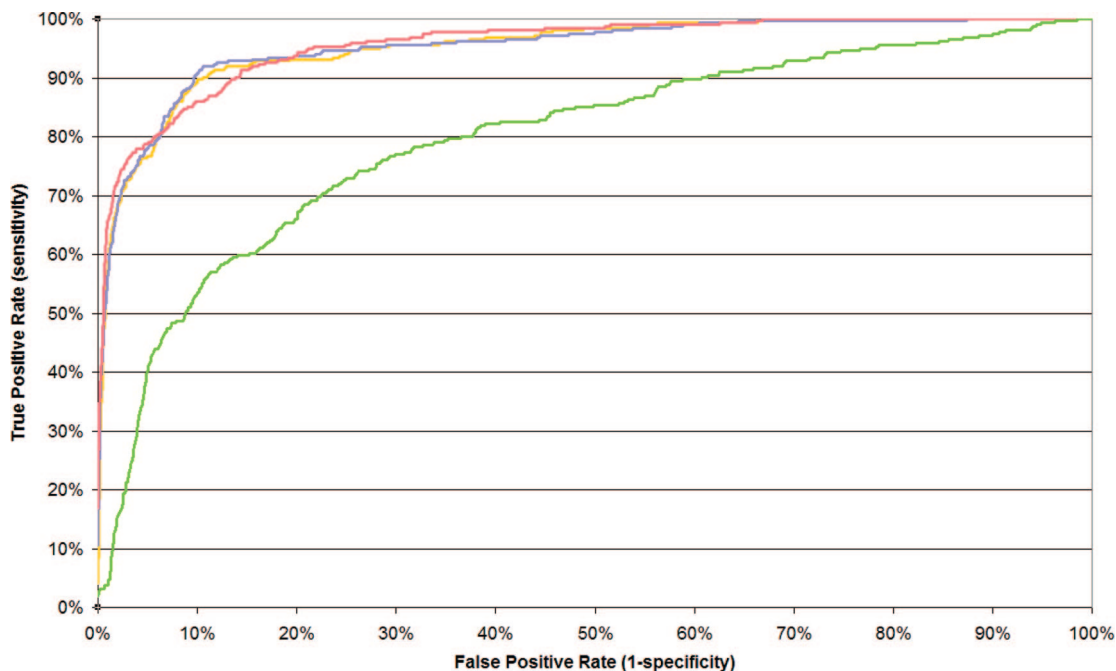


**Figure 3.** ROC curves based on the validation results of SSP 1 (green), 2 (orange), 3 (blue), and 4 (red).

chemical groups such as ester moieties located in the middle of the compound scaffold were discarded. Moreover, compounds containing substructures, which are known to cause low bioavailability, metabolic instability, and side effects because of competing reactions *in vivo*, were excluded. For example, compounds containing electrophilic warhead groups such as  $\alpha$ -haloketones, 1,2-dicarbonyls, and aldehydes, could be added to nucleophiles (e.g., serum proteins and glutathione) *in vivo* and therefore were not selected for biological testing.<sup>27</sup> Then 305 structurally diverse compounds were selected. Consequently, these compounds were aligned to the corresponding PPAR agonist pharmacophore model within LigandScout to visually investigate the pharmacophore feature alignment and to exclude false positives with in terms of PPAR agonist-likeness implausible feature mapping. For instance, compounds with a strongly hydrophilic headgroup, such as a carboxylic acid moiety, were regarded to be more likely a PPAR agonist than a compound that contained a nitro headgroup and therefore could only form a weak hydrogen bond network with the active site residues.<sup>28</sup> Because we searched for new scaffolds for PPAR agonists, we determined the structural distance of the remaining virtual screening hits to the 321 PPAR agonists of the PPAR ligand test set using our Pipeline Pilot script for structural similarity analysis. Only compounds were kept that did not form a cluster with any of the 321 known PPAR agonists at a maximum allowed Tanimoto dissimilarity of 0.7. Finally, the SciFinder database<sup>29</sup> was searched for PPAR activity reported for the compounds, which was another hit exclusion criterion. From the remaining 21 compounds, 10 were available for purchase (Chart 1).

To avoid testing of a compound that represents a simple derivative of a common scaffold for PPAR agonists, the 10 compounds were subjected to a SciFinder database similarity search using a Tanimoto score cutoff  $\geq 80$ . Only for compound **4**, structurally similar PPAR ligands were retrieved. However, the thiazolidine derivatives, which received a Tanimoto score of 90, were reported as PPAR antagonists by Shen et al.<sup>30</sup> These PPAR antagonists possessed a phenoxy acetic acid moiety similar to the hydrophilic headgroup of known PPAR agonists.<sup>31</sup> On that account, we did not exclude that compound **4**, which is

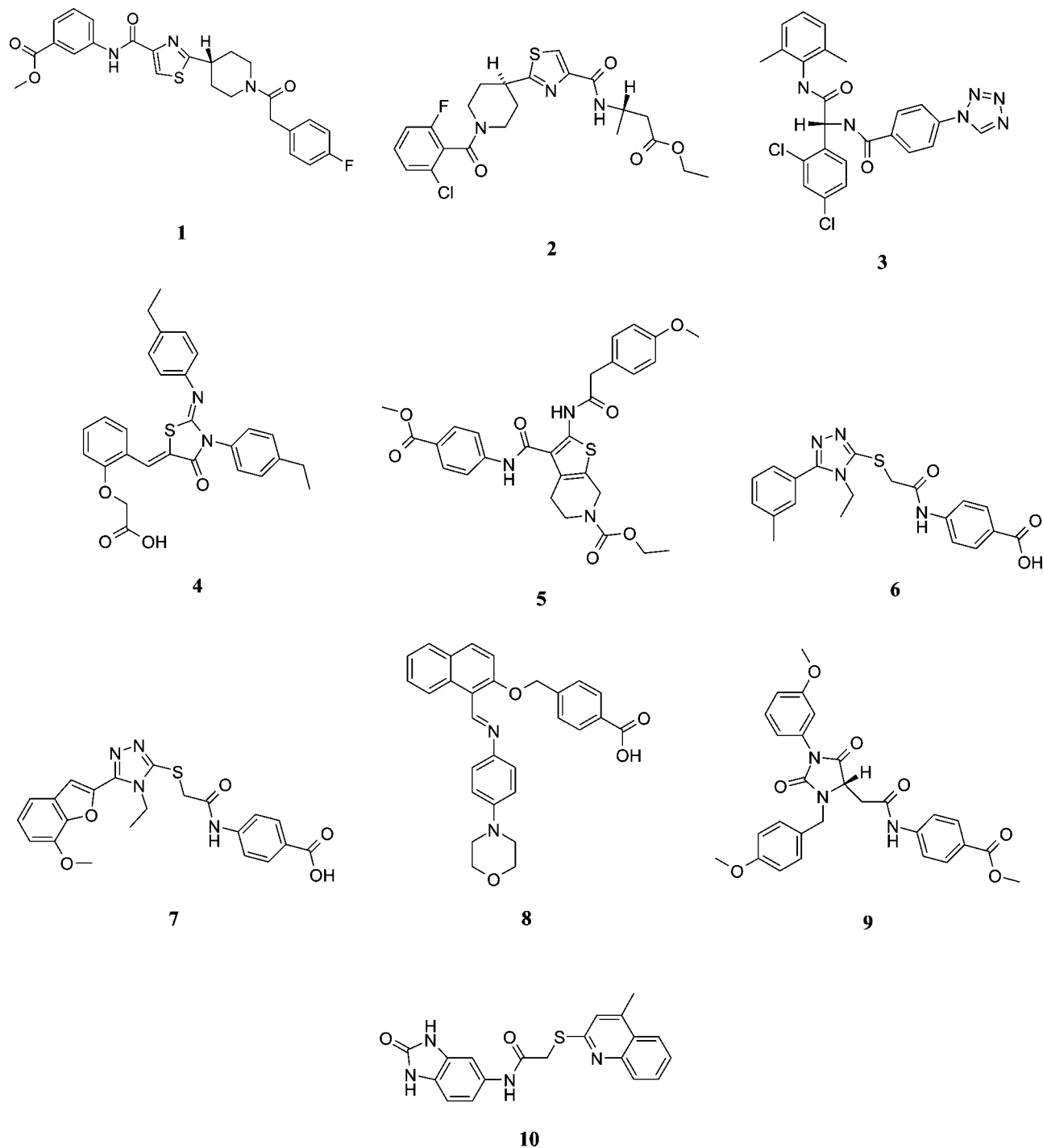
a derivative of these thiazolidines, is able to exert agonistic activity at one PPAR subtype. Thus, we also measured the biological activity of this compound.

Compounds **6** and **7** are structurally closely related. To investigate the difference in PPAR activity between a ring system, which contains a hydrogen bond accepting ether oxygen, and a hydrophobic moiety, which is not able to form any hydrogen bond, both were selected for biological testing.

**Biological Testing of Virtual Screening Hits.** The selected 10 compounds were biologically tested for PPAR activity using cell-based hPPAR-LBD transactivation assays. For each of the three PPAR subtypes a transactivation assay was set up in order to determine the selectivity of the compounds in activating PPAR- $\alpha$ , PPAR- $\gamma$ , and PPAR- $\delta$ . Five out of ten compounds were able to activate one of the PPAR subtypes at 10  $\mu\text{M}$ : (i) compounds **5**, **7**, and **8** activated PPAR- $\alpha$ , (ii) compound **9** showed agonistic activity for PPAR- $\gamma$ , (iii) compound **2** caused a significant transactivation response in both the hPPAR- $\alpha$ -LBD and hPPAR- $\gamma$ -LBD transactivation assay. Compound **5**, the most potent PPAR- $\alpha$  agonist among the compounds, induced an activation of PPAR- $\alpha$  at 10  $\mu\text{M}$ , which is comparable to about 40% of the PPAR activity measured for the positive control GW7647. At 10  $\mu\text{M}$ , compounds **7** and **8** were both able to cause an activation of PPAR- $\alpha$  of approximately 15% of the positive control activity. Surprisingly, compound **6**, a tolyl derivative of compound **7**, did not cause a significant transactivation response in any of the three hPPAR-LBD assays at 10  $\mu\text{M}$ . The most potent PPAR- $\gamma$  agonist, compound **9**, induced a response in the hPPAR- $\gamma$ -LBD transactivation assay at 10  $\mu\text{M}$  comparable to about 20% of the PPAR- $\gamma$  activity measured for the positive control rosiglitazone. For compound **2**, a PPAR- $\alpha$  activation of about 20% and a PPAR- $\gamma$  activation of about 15% of the positive control activity at 10  $\mu\text{M}$  was detected (Figure 4).

The results of the hPPAR-LBD transactivation assays for compounds **2**, **5**, **7**, **8**, and **9** reported as fold activation of PPAR compared to an untreated cell at concentrations of 0.1, 1, and 10  $\mu\text{M}$  are displayed in Table 2.

None of the ten compounds showed a significant activity in the hPPAR- $\delta$ -LBD agonist transactivation assay.

**Chart 1.** Structures of the 10 Compounds Biologically Tested for PPAR activity

Although the virtual screening workflow was designed to identify PPAR agonists, it was observed that compound **9** was able to repress the activity of the hPPAR- $\delta$ -LBD in a dose-dependent manner (data not shown). Accordingly, compound **9** was also tested for the ability to dose-dependently antagonize the transactivation response caused by the positive control L165041. Compound **9** was identified as a potential PPAR- $\delta$  antagonist because it repressed the basal activity of hPPAR- $\delta$ -LBD and was able to reduce transcriptional activity induced by the positive control L165041 in the hPPAR- $\delta$ -LBD by about half at a concentration of 1  $\mu$ M (Figure 5).

Afterward, the  $IC_{50}$  values of the five active compounds were measured using a competitive binding assay as described in the Experimental Section. The observed dose-response

curves and  $IC_{50}$  values are presented in Figure 6 and Table 3, respectively.

In general, the binding data corresponded with the activity pattern of the five compounds observed in the hPPAR-LBD transactivation assays. Compounds **5** ( $IC_{50} = 1.5 \mu$ M) and **7** ( $IC_{50} = 1.0 \mu$ M) were identified as PPAR- $\alpha$  ligands, whereas compound **8** ( $IC_{50} = 43 \mu$ M) was a very weak PPAR- $\alpha$  ligand. Compounds **2** ( $IC_{50} = 44 \mu$ M) and **9** ( $IC_{50} = 13 \mu$ M) were able to bind to PPAR- $\gamma$ . In addition, as expected, compound **9**, which repressed the positive control activity in the hPPAR- $\delta$ -LBD assay, possessed binding affinity for PPAR- $\delta$ . However, some unexpected binding affinity data was obtained: (i) compound **2** did not bind to PPAR- $\alpha$ , although it caused a significant response in the hPPAR- $\alpha$  transactivation assay, (ii)

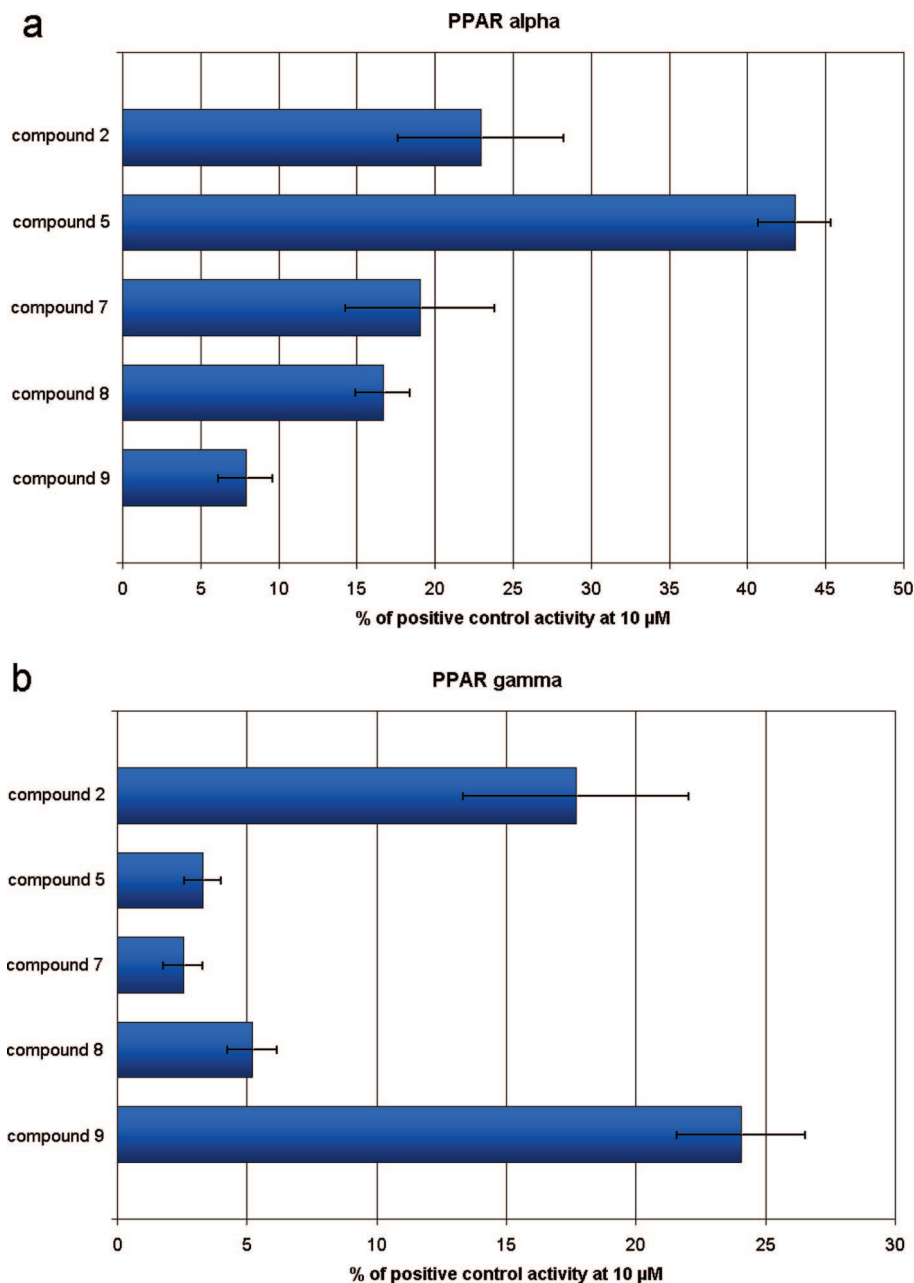


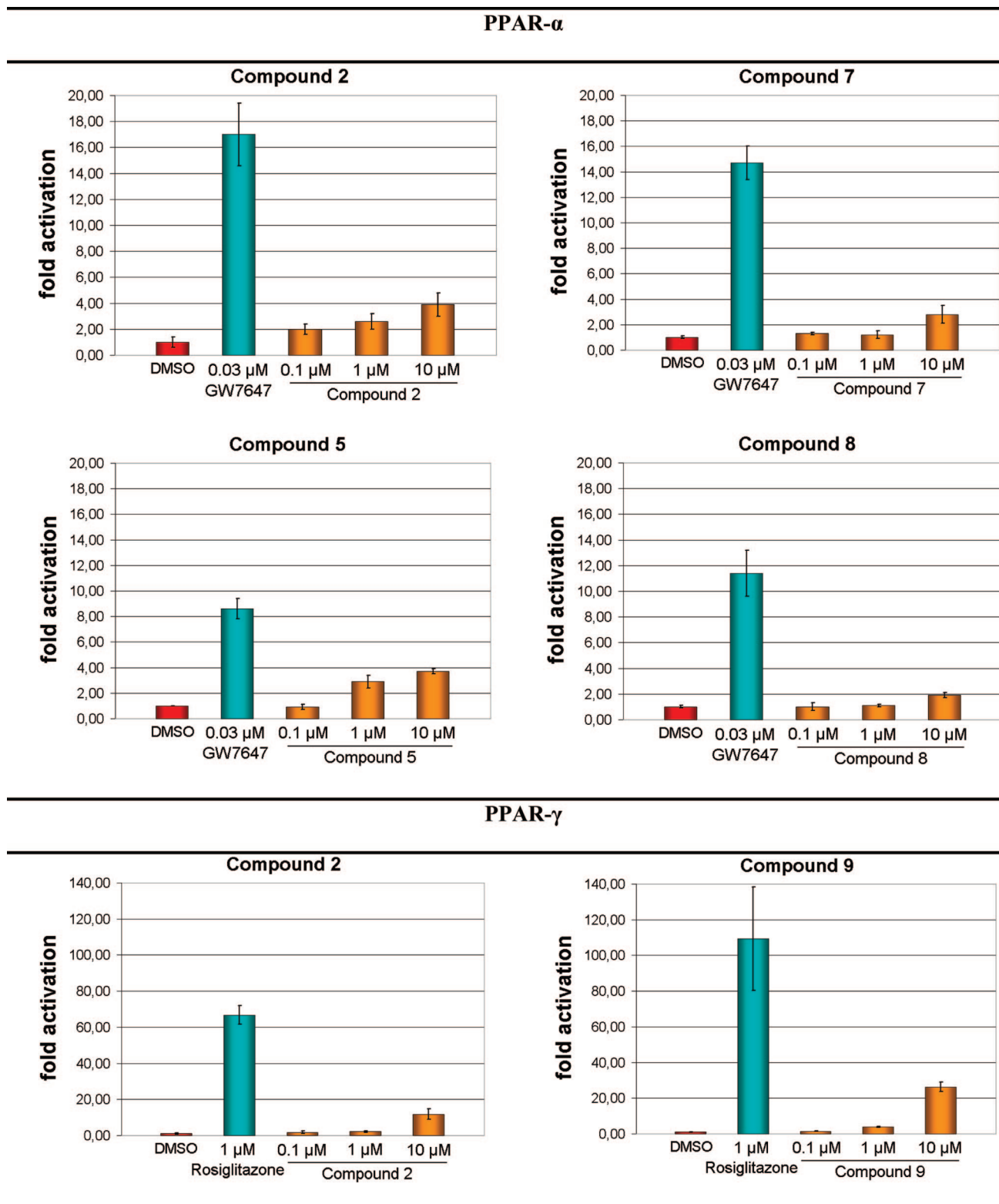
**Figure 4.** hPPAR- $\alpha$ -LBD (a) and hPPAR- $\gamma$ -LBD (b) transactivation assay results for compounds **2**, **5**, **7**, **8**, and **9**. PPAR activation was measured using human GAL4-PPAR chimeric receptors and a luciferase reporter gene expressed in Hepa 1-6 (hPPAR- $\alpha$ -LBD transactivation assay) and MEFs (hPPAR- $\gamma$ -LBD and hPPAR- $\delta$ -LBD transactivation assay). The compound activity determined at 10  $\mu$ M is expressed as percentage of the PPAR activity detected for the positive control. GW7647 and rosiglitazone served as positive control for the hPPAR- $\alpha$ -LBD and hPPAR- $\gamma$ -LBD transactivation assay, respectively.

compounds **7** and **8**, which were identified as selective PPAR- $\alpha$  activators in the transactivation assay, displayed weak binding affinity for PPAR- $\gamma$  ( $IC_{50}$  = 40  $\mu$ M and  $IC_{50}$  = 20  $\mu$ M), (iii) compound **8** was able to bind to PPAR- $\delta$  ( $IC_{50}$  = 34  $\mu$ M) without inducing gene transcription.

**Docking of Novel PPAR Ligands.** The five novel PPAR agonists **2**, **5**, **7**, **8**, and **9** were docked to the corresponding PPAR ligand-binding pocket in order to determine their putative binding mode. As described in the Experimental Section, the ligand-binding pocket of PDB entry 1k7l was used for docking studies on the PPAR- $\alpha$  agonists **5**, **7**, and **8**. In contrast to that, the PPAR- $\gamma$  activators **2** and **9** were docked to the ligand-binding pocket extracted from the PDB complex 2f4b. For the putative binding mode of compound **5**, two hydrogen bonds between the carboxyl oxygen of the ethyl ester moiety of the

compound and residues Tyr314 and Ser280 were determined. In addition, hydrophobic interactions established between the ethyl ester moiety and residues Phe273, Val444, Leu456, and Leu460, between the phenoxy moiety and residues Ile272, Met330, Val332, Ile339, and Leu344, as well as between the phenyl ring adjacent to the methyl ester group, and residues Thr279, Leu321, and Val332, were detected (Figure 7a).

Afterward, the putative binding modes of the structurally closely related compounds **6** (Figure 7b) and **7** (Figure 7c) were investigated to rationalize the lack of PPAR activity measured for compound **6**. For compound **7**, a binding mode was predicted that includes three hydrogen bonds formed between the carboxylic moiety of the compound and the three active site residues Ser280, Tyr314, and Tyr464. Another hydrogen bond was established between the methoxy group adjacent to the

**Table 2.** Fold PPAR Activation of Compounds 2, 5, 7, 8, and 9 and of the Positive Control in Comparison to Untreated Cells

benzofuran moiety and residue Thr279. A  $\pi$ - $\pi$  interaction was predicted between the phenyl ring adjacent to the carboxylic acid and residue His440. In addition, hydrophobic contacts between the latter phenyl ring and residue Ile354, between the ethyl moiety of the triazole ring and residues Tyr279, Leu321, Met330, and Val332, and between the benzofuran moiety and residues Ala333 and Tyr334, were predicted. A similar binding mode was predicted for compound 6. However, no

hydrogen bond could be formed between compound 6 and residue Thr279.

The best docking pose for the weak PPAR- $\alpha$  agonist 8 showed two hydrogen bonds located between the carboxyl moiety and residue Tyr314, as well as one hydrogen bond formed between this carboxyl group and residue Ser280 and another hydrogen bond situated between the morpholine oxygen and residue Ser280 (Figure 7d). The ring moieties of compound



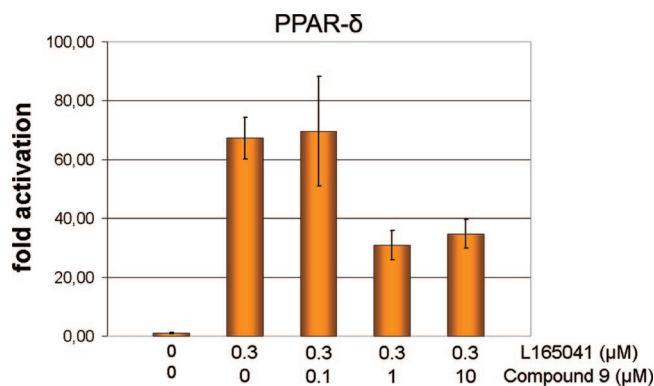


**Figure 5.** Dose-dependent attenuation of the positive control activity in the PPAR- $\delta$ -LBD transactivation assay by compound **9**.

**Table 3.** IC<sub>50</sub> Values Calculated for the Five Compounds Which Caused a Response in the Transactivation Assay

PPAR subtype	IC <sub>50</sub> (μM) <sup>a</sup>				
	compound				
	2	5	7	8	9
PPAR- $\alpha$		1.5	1.0	43	
PPAR- $\gamma$	44		40	20	13
PPAR- $\delta$			390	34	7.2

<sup>a</sup> IC<sub>50</sub> values were determined by linear regression analysis of dose-response curves using the GraphPad Prism program.

**8** were predicted to be involved in hydrophobic interactions with residues Ile272, Phe273, Thr279, Thr283, Ile317, Phe318, Leu321, Leu344, Phe351, Ile354, Met355, Val444, Ile447, and Leu456.

For the binding mode of compound **2**, two hydrogen bonds located between the carbonyl oxygen of the ester moiety and residues His449 and Tyr473 were predicted (Figure 8a).

Furthermore, hydrophobic interactions were formed between the ethyl ester moiety and residues Phe282, Leu453, Leu465, Leu469, and Tyr473, between the butanoic acid moiety and residue Phe282, between the thiazole ring and residues Ile326 and Leu330, as well as between the 2-chloro-6-fluorophenyl moiety and residues Ile281, Ile341, and Met348.

When compound **9** was docked to the PPAR- $\gamma$  ligand-binding pocket, a hydrogen bond located between the ester moiety of the PPAR- $\gamma$  agonist and the active site residue Tyr473 was detected (Figure 8b).  $\pi$ - $\pi$  interactions were predicted between the phenyl ring adjacent to the ester moiety and residue His449, as well as between the *p*-methylphenoxy ring and residue Arg288. Furthermore, the predicted binding mode includes hydrophobic interactions between the phenyl group adjacent to the ester moiety and residue Ile326, between the *p*-methylphenoxy ring and residues Leu333 and Ile341, and between the phenoxy ring and residues Ile281, Val339, Ile341, Met348, Leu353, and Met364.

Finally, to explain the antagonistic PPAR- $\delta$  activity of compound **9**, an induced fit docking study was performed (see Experimental Section). For this purpose, compound **9** was docked to the ligand-binding pocket of the PDB entry 2awh. Compound **9** was predicted to form hydrophobic interactions between the *m*-methoxyphenyl moiety and residues Thr288 and Ile333, between the *p*-methoxyphenyl moiety and residues Val281, Val341, Val348, and Leu353, and between the phenyl ring adjacent to the ester and residues Thr289, Phe327, Ile363, and Met453. A significant increase in size of arm I of the PPAR- $\delta$  ligand-binding pocket of the protein modified by induced fit docking (Figure 9a) compared to arm I of the ligand-

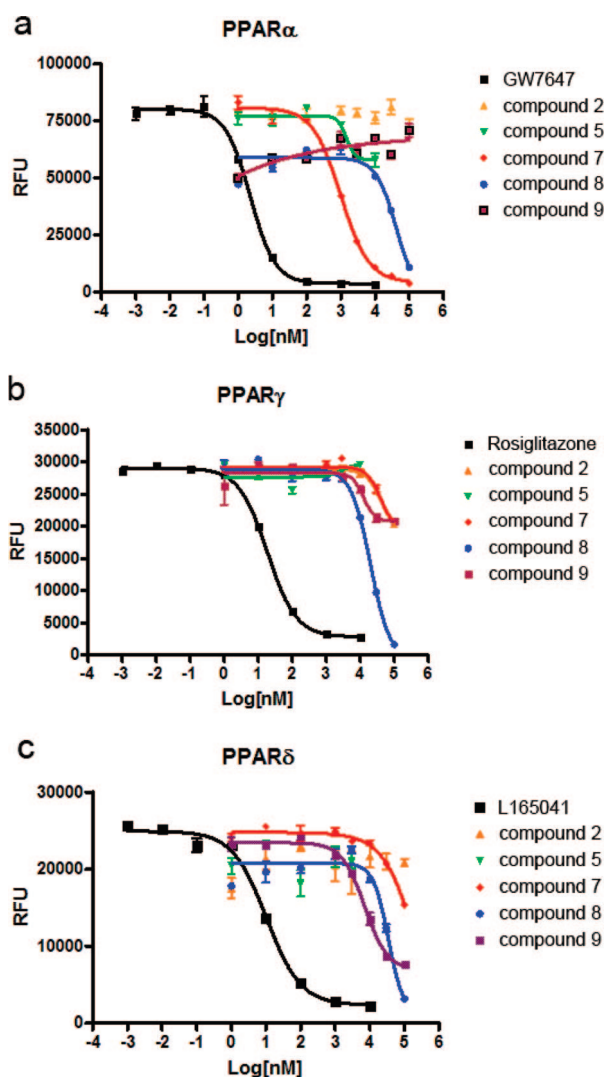


**Figure 6.** Dose-response curves obtained for compounds **2**, **5**, **7**, **8**, and **9** in a competitive binding assay. As described in the Experimental Section, the displacement of a fluorescent pan PPAR agonist from the PPAR- $\alpha$  LBD (a), PPAR- $\gamma$  LBD (b), and PPAR- $\delta$  LBD (c) by the compound was measured and expressed as RFU value, respectively.

binding pocket of the original protein from PDB entry 2awh (Figure 9b) was observed.

Visualization of the induced fit docking pose for compound **9** within the original protein showed that the carboxylic ester moiety of the PPAR- $\delta$  antagonist penetrates through arm I of the ligand-binding pocket. Thus, antagonistic activity could be explained by the displacement of residues of arm I, which could inhibit the stabilization of the active conformation of the AF2-helix as known for other PPAR antagonists.<sup>15</sup>

## Discussion

To discover new scaffolds for PPAR agonists, we combined 3D pharmacophore-based screening with 3D shape and electrostatic similarity search techniques to screen commercial libraries. The four best PPAR agonist models described in our previous study (see ref 21 for more details) served as queries for the pharmacophore modeling part of our virtual screening approach. The physicochemical properties of the resulting virtual screening hits were analyzed by executing a Pipeline Pilot script. The compounds, which matched the filter criteria derived from the physicochemical properties of the 321 PPAR agonists of the PPAR ligand test set, were subjected to 3D shape and

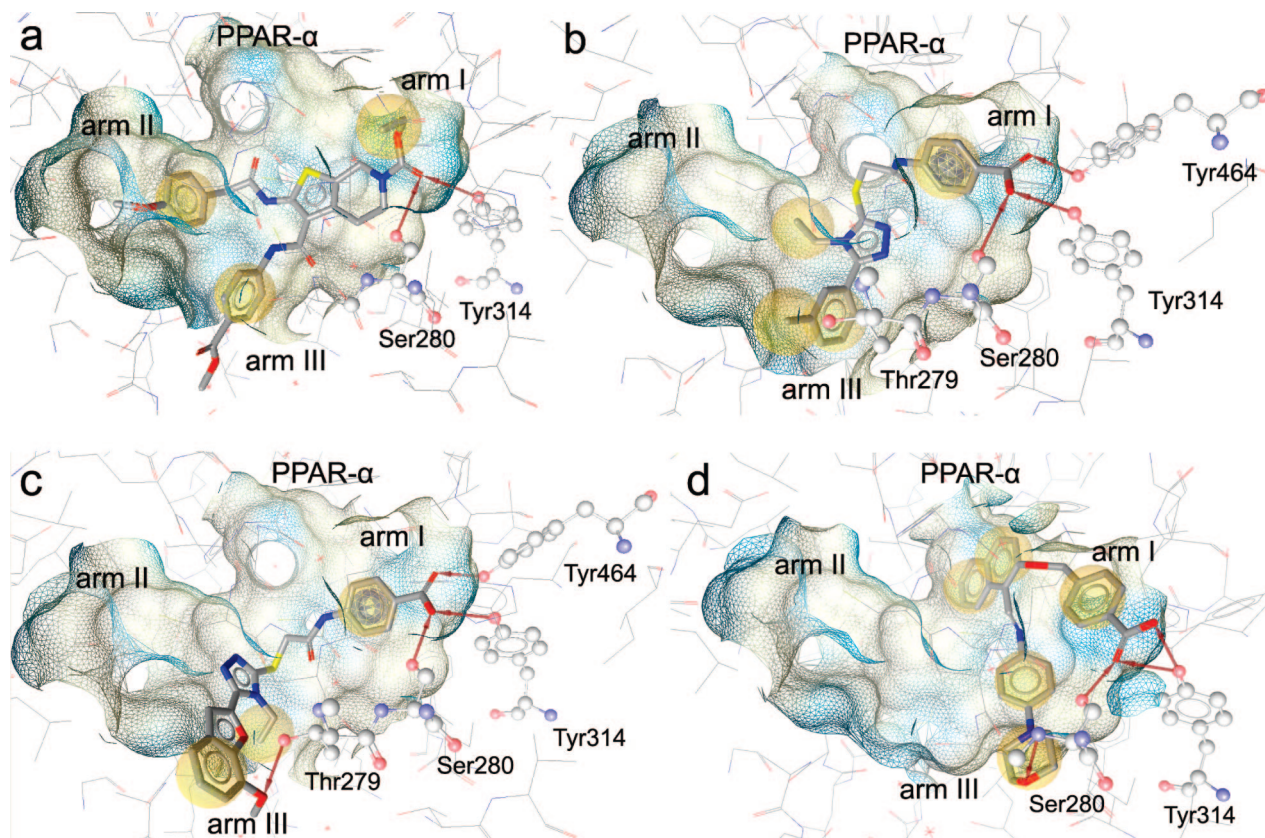


**Figure 7.** Putative ligand–protein interactions of compounds **5** (a), **6** (b), **7** (c), and **8** (d). Gold was used to dock the biologically inactive compound **6**, as well as the three PPAR- $\alpha$  agonists **5**, **7**, and **8** to the ligand-binding pocket of PPAR- $\alpha$ . The calculated docking poses were analyzed and visualized utilizing LigandScout. Red arrows show hydrogen bond acceptors, hydrophobic interactions are displayed by yellow spheres, and a wireframe colored by lipophilicity represents the surface of the PPAR ligand-binding pocket.

electrostatic similarity screening. The three PPAR agonists on which our best structure-based pharmacophore models are based and the PPAR activator used for deriving the Catalyst shape of our most selective ligand-based pharmacophore model served as query molecules for four SSPs. The four SSPs were validated by screening the 321 PPAR agonists and a virtual database containing 12775 PPAR decoys to determine the protocol with the highest discriminatory power for our virtual screening workflow. Because ROC curve analysis of the validation results indicated that SSP 2, 3, and 4 cannot be ranked with respect to their discriminatory power, all three protocols were included in our virtual screening workflow. The virtual screening hits of the 3D shape and electrostatic similarity screening were clustered according to their structural similarity and visually investigated in terms of chemical stability and PPAR agonist lead-likeness. For the remaining compounds, the structural distance to the 321 PPAR agonists of the PPAR ligand test set was determined in order to not subject compounds to biological testing that were structurally similar to known PPAR agonists. Finally, a Sci-Finder database search was performed to see if the remaining compounds were reported as PPAR agonists in literature and consequently to discard these compounds. This virtual screening workflow resulted in 10 compounds, which were biologically tested using hPPAR-LBD transactivation assays and a competitive binding assay.

Compounds **5**, **7**, and **8** induced gene transcription in the hPPAR- $\alpha$ -LBD transactivation assay and showed binding affinity for PPAR- $\alpha$  in the low micromolar range. Thus, these compounds were identified as PPAR- $\alpha$  agonists. Interestingly, compound **6**, which differs from compound **7** only in the *m*-tolyl moiety adjacent to the 1H-1,2,4-triazole ring, shows no signifi-

cant activity at any PPAR subtype. Therefore, the 7-methoxy-benzofuran moiety of compound **7** seems to be essential for PPAR- $\alpha$  activation. On the basis of the results of the binding and transactivation assay compound **2** acts as a PPAR- $\gamma$  agonist. However, compound **2** also exerted activity in the hPPAR- $\alpha$ -LBD transactivation assay, which did not correspond with the lack of binding affinity for PPAR- $\alpha$ . Some PPAR agonists, which contain an ester moiety, especially activators of the  $\alpha$ -subtype, are known to be hydrolyzed *in vivo* to the biological active carboxylic acid metabolite.<sup>32</sup> On that account, the unesterified metabolite could represent the active form of compound **2**. Because the transactivation assay but not the binding assay is cell-based and therefore comprises enzymes that are able to hydrolyze the ester moiety of compound **2**, this active metabolite would only be formed in the transactivation assay and would be absent in the binding assay, which could be an explanation for the observed biological data. Whether this is true or not has to be determined in future studies. Compound **9** caused only a transactivation response in the hPPAR- $\gamma$ -LBD assay but showed binding affinity for both PPAR- $\gamma$  and PPAR- $\delta$ . When the compounds were tested for possible antagonistic activity in the transactivation assay, compound **9** was able to attenuate the activity of the PPAR- $\delta$  positive control in a dose-dependent manner and repress the basal activity of hPPAR- $\delta$ -LBD. Taking this into consideration, compound **9** was identified as both a PPAR- $\gamma$  agonist and a possible PPAR- $\delta$  antagonist. For PPAR antagonism, a bulky moiety is needed that displaces active site residues and thereby moves the AF-2 helix into a position that enables the binding of corepressor proteins.<sup>15</sup> PPAR agonists containing a bulky moiety that fits perfectly to the large ligand-binding pocket of the active conformation of PPAR- $\alpha$

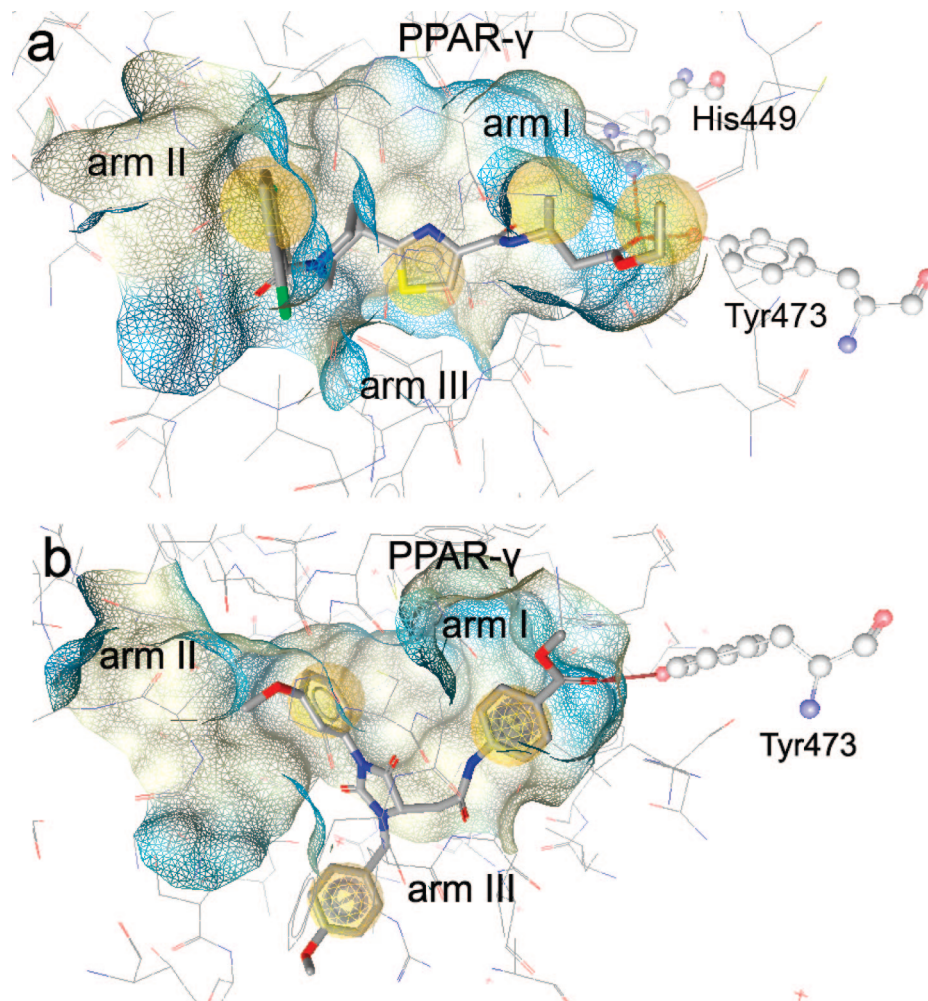


**Figure 8.** Putative binding mode of the two PPAR- $\gamma$  agonists **2** (a) and **9** (b).

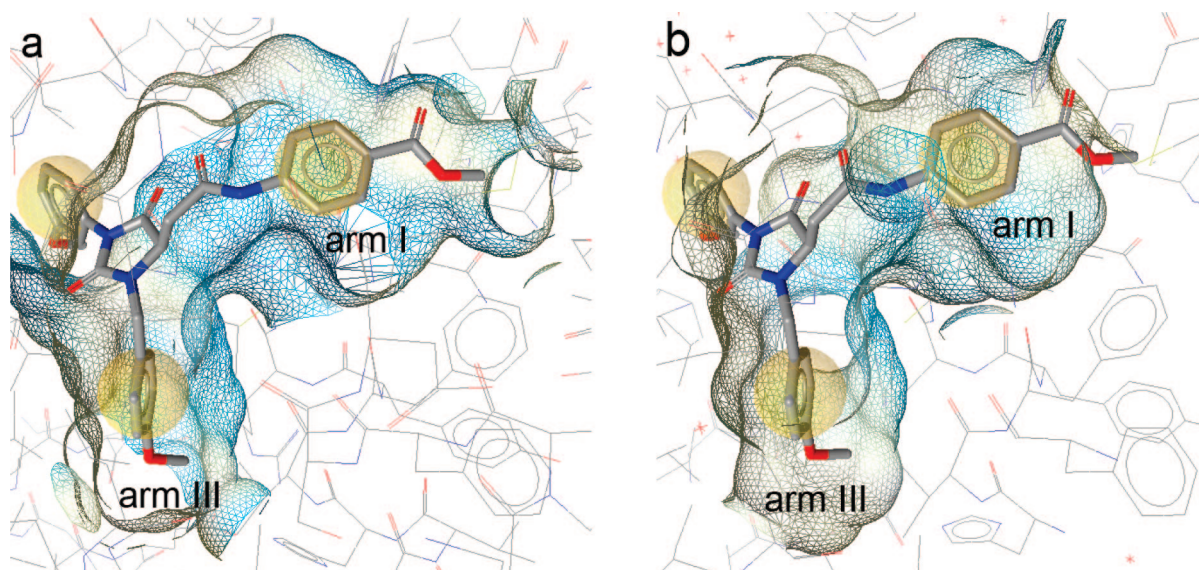


**Figure 9.** PPAR- $\delta$  antagonist **9** docked to the protein by induced fit docking (a) and the same docking pose for compound **9** inserted into the ligand-binding pocket of the original protein of PDB entry 2awh (b). Movement of ligand-binding pocket residues caused by induced fit docking led to a significant increase in size of arm I compared to the original ligand-binding pocket. This displacement of residues of arm I by compound **9** could be an explanation for its PPAR- $\delta$  antagonistic activity.

or PPAR- $\gamma$  but is too bulky to allow the stabilization of the active conformation of PPAR- $\delta$ , could cause a displacement of active site residues within the substantially smaller PPAR- $\delta$  ligand-binding pocket and thus inhibit PPAR- $\delta$  activation.

Moreover, a compound with both PPAR- $\gamma$  agonistic and PPAR- $\delta$  antagonistic activity has already been reported in literature.<sup>5</sup> On that account, a virtual screening workflow that is focused on scaffold hopping for PPAR agonists for all three

subtypes, will not exclude antagonists that are structurally related to agonists or also exert agonistic activity for another PPAR subtype. Therefore, although our virtual screening workflow was designed to discover PPAR agonists, the discovery of a possible PPAR- $\delta$  antagonist with also agonistic activity for PPAR- $\gamma$ , such as compound **9**, was not unexpected.

None of the 10 compounds showed significant PPAR- $\delta$  agonistic activity. Due to the absence of biologically active PPAR- $\delta$  agonists, we evaluated the performance of our virtual screening workflow for enriching PPAR- $\delta$  agonists. For this purpose, we screened a database consisting of 17 selective PPAR- $\delta$  agonists of the PPAR ligand test set and of 12775 PPAR decoys from the virtual database. The 3D pharmacophore-based screening, physicochemical property filtering, and 3D shape and electrostatic similarity screening resulted in five out of 17 selective PPAR- $\delta$  agonists (29%) and four out of 12775 PPAR decoys (0.03%). Taking these results into account, an enrichment factor of 418 was calculated, which means that the virtual screening workflow performs 418 times better in discriminating PPAR- $\delta$  agonists from decoys than a random compound selection. Assuming that we did not exclude a large number of potential PPAR- $\delta$  agonists by structural similarity analysis and visual inspection, the lack of biological tested PPAR- $\delta$  agonists can be rather explained by the limited chemical space of the commercial library compounds than by an insufficient discriminatory power of our virtual screening workflow for PPAR- $\delta$  agonists.

To explain the agonistic activity of compounds **2**, **5**, **7**, **8**, and **9**, the structures were docked to the PPAR- $\alpha$  and PPAR- $\gamma$  ligand-binding pocket, respectively. Thereafter, the putative binding mode of the best docking pose of each compound was determined. The predicted binding modes of all compounds include hydrogen bonds to the active site residues, as well as hydrophobic contacts to each of the three arms of the PPAR ligand-binding pocket. Furthermore, we also investigated the putative binding mode of the biological inactive compound **6**. Thus, we tried to explain the observed difference in PPAR activity between compound **6** and the structurally closely related PPAR- $\alpha$  agonist **7**. An analysis of the resulting docking poses indicated that the major difference between the putative binding modes of both compounds is a hydrogen bond to residue Thr279. This hydrogen bond is only formed by the methoxy group of the benzofuran moiety of the docked compound **7**. Hydrogen bonds to residue Thr279 have been reported for the ligand-binding mode of PPAR- $\alpha$  agonists.<sup>33</sup> Therefore, the lack of PPAR activity determined for compound **6** could be explained. Finally, an induced fit docking of the PPAR- $\gamma$  agonist and possible PPAR- $\delta$  antagonist **9** to PPAR- $\delta$  was performed to predict an antagonistic binding mode. The results showed that an antagonistic activity could be related to the displacement of residues in the area of arm I of the PPAR- $\delta$  ligand-binding pocket by compound **9**.

## Conclusion

We showed that a virtual screening approach based on the combined use of pharmacophore modeling, 3D shape, and electrostatic similarity screening can be used to discover novel scaffolds for PPAR ligands. Five out of ten virtual screening hits exerted PPAR activity. Based on binding and transactivation data compounds **5**, **7**, and **8** act as PPAR- $\alpha$  agonists, compound **2** represents a novel PPAR- $\gamma$  agonist, and compound **9** was identified as both a PPAR- $\gamma$  agonist and a possible PPAR- $\delta$  antagonist. On that account, it was proven that a combination of pharmacophore modeling with 3D shape and electrostatic

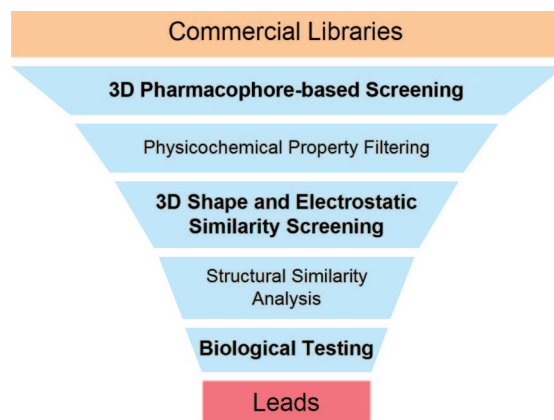


**Figure 10.** Virtual screening workflow.

**Table 4.** Structure-Based Pharmacophore Models Were Derived from 21 PDB Entries

agonist-PPAR- $\alpha$ complex	agonist-PPAR- $\gamma$ complex	partial agonist-PPAR- $\gamma$ complex	agonist-PPAR- $\delta$ complex
1i7g	1fm6	1zeo	1gwx
1k7l	1fm9	2fvj	1y0s
	1i7i	2g0g	2g0g
	1k74	2g0h	2g0h
	1knu	4prg	4prg
	1nyx		
	1wm0		
	2f4b		
	2prg		

similarity search techniques enriches novel scaffolds for PPAR ligands. Finally, a docking study was performed to explain the activity of the novel PPAR ligands **2**, **5**, **7**, **8**, and **9**, which could be structurally optimized in order to obtain new drugs for the therapy of atherosclerosis, dyslipidaemia, and type 2 diabetes.

## Experimental Section

**Hardware Specifications.** An Intel Pentium Core 2 Duo 6400 equipped with 1 GB RAM running Linux Fedora Core 6 was utilized for performing the molecular modeling studies.

**Virtual Screening Workflow.** An overview of our virtual screening workflow is displayed in Figure 10.

**Pharmacophore Modeling.** For the generation of structure-based pharmacophore models for PPAR- $\alpha$ , PPAR- $\gamma$ , and PPAR- $\delta$  agonists, the software LigandScout was applied. The ligand–protein interactions of 21 PPAR agonist–protein complexes found in the PDB were investigated and a pharmacophore model for each PDB entry was derived (Table 4).

In addition, several ligand-based pharmacophore models were created by using compound sets of potent and structurally diverse PPAR agonists as input for the HipHop algorithm implemented in the software package Catalyst. The resulting structure-based and ligand-based models were refined and validated within Catalyst. For model refinement, training sets containing PPAR agonists and the Derwent World Drug Index 2003<sup>34</sup> were utilized, whereas the selectivity of the refined models was determined by screening a large test set consisting of 357 PPAR ligands (321 PPAR agonists and 36 PPAR inactives derived from literature, Table 5) and a virtual database of 12775 PPAR decoys. The latter was generated using the Java-based software ilib:diverse<sup>35</sup> in order to calculate the corresponding enrichment factors for the pharmacophore models.

For more details about the model generation and validation process and the compilation of the different PPAR compound sets, see ref 21. A detailed description of the virtual database generation can be found in ref 24. With respect to the validation results, the

**Table 5.** Composition of the PPAR Ligand Test Set

classification	number
PPAR agonists	321
PPAR- $\alpha$ agonists	31
PPAR- $\alpha$ / $\gamma$ agonists	88
PPAR- $\alpha$ / $\delta$ agonists	20
PPAR- $\gamma$ agonists	135
PPAR- $\gamma$ / $\delta$ agonists	1
PPAR- $\gamma$ partial agonists	5
PPAR- $\delta$ agonists	17
PPAR pan agonists	24
PPAR inactives	36

best pharmacophore models for PPAR- $\alpha$ , PPAR- $\gamma$ , and PPAR- $\delta$  agonists were selected and used as queries for a virtual screen of commercial libraries.

**Virtual Screening of Commercial Libraries.** Conformational models for the commercial library compounds were created using the conformer generating algorithm of Catalyst-ConForm with the following settings: Maximum number of conformers = 100, generation type = fast quality, and energy range = 20 kcal/mol above the calculated lowest energy conformation. 3D pharmacophore-based virtual screening of commercial libraries was performed by applying Catalyst default settings except for the following screening parameters: (i) the parameter that describes the distance between features, compare.minInterBlobDistance, was set to 0 in order to place pharmacophore model features closely on a compound, (ii) to enable that phenyl sulfonamide moieties match hydrophobic features also the FunctionMapping.Hydrophobe.Neighbor.numBondLessEqualFromOWithDoubleBond parameter was adjusted to 0. A fluorine hydrogen bond donor feature according to Wolber et al.<sup>17</sup> was imported into the default Catalyst feature dictionary. For 3D database screening, Catalyst contains two search algorithms. The Fast Flexible Search algorithm utilizes the input conformers of the compound to match the pharmacophore model features. In contrast to that, the exhausting Best Flexible Search algorithm generates additional conformers to improve the alignment between compound and pharmacophore model. Because the Fast Flexible Search algorithm is more suitable for screening large databases, it was executed for the virtual screen of commercial libraries. Catalyst considers only compounds as virtual screening hits that match all pharmacophore model features. The resulting virtual screening hits were scored by the fit value calculated within Catalyst. The fit value is determined by the feature mapping and the corresponding feature weight. If the default feature weight of 1 is used and the feature maps perfectly, a fit value of 1 is calculated. Compounds that do not exactly match the feature center get a fit value lower than 1. The fit value for a compound aligned with a pharmacophore model is equivalent to the sum of the single feature fit values. Depending on the executed Catalyst search algorithm, Fast Fit and Best Fit values are calculated, respectively. Therefore, our virtual screening hits were scored by the Fast Fit value.

#### Physicochemical Property Filter for Virtual Screening Hits.

The virtual screening hits that resulted from the pharmacophore modeling approach were filtered with respect to their physicochemical properties by utilizing a Pipeline Pilot script.<sup>36</sup> The filter criteria were derived from the physicochemical property distribution of the 321 PPAR agonists of the PPAR ligand test set described in ref 21. The physicochemical properties of the 321 PPAR agonists were analyzed within the software package MOE.<sup>37</sup> The following filter criteria were applied: (i) the minimum and maximum of the molecular weight was set to 300 and 600 Da, respectively, (ii) the maximum for the AlogP value was adjusted to 7, (iii) the number of heavy atoms was limited to 20–40, (iv) at least 4 and at maximum 10 atoms of the compound had to be a nitrogen or an oxygen, (v) the number of hydrogen bond acceptor atoms was allowed to range from 3 to 7, whereas the number of hydrogen bond donors was restricted to 1–3. The remaining compounds were exported as MDL SD-file and subjected to the 3D shape and electrostatic similarity screening approach.

**3D Shape and Electrostatic Similarity Screening.** Openeye's software ROCS<sup>38</sup> aligns molecules by a volume overlap maximization technique. The software EON<sup>39</sup> determines the electrostatic potentials of two compounds and consequently calculates the Electrostatic Tanimoto coefficient between these two molecules. Both algorithms were used for our virtual screening approach. For conformational analysis of compounds, the default settings of Openeye's conformational model generator Omega<sup>40</sup> were applied. The resulting set of multiconformer compounds was stored in the OEBinary v2-file format and served as input for ROCS calculations. For this purpose, the default settings of ROCS were applied, except for the parameter eon\_input\_size, which was changed from 1000 to 0 in order to align not only the best 1000 molecules ranked by ROCS but all molecules of the focused compound library to the query molecule. The resulting aligned OEBinary v2-file served as EON input database. The EON parameter besthits was set to 1500. Therefore, only the top-ranked 1500 molecules were written to the EON output MDL SD-file. All other parameters were default. In the default settings EON ranks input molecules by using the Electrostatic Tanimoto combo score (ET\_combo), which represents the sum of Poisson–Boltzmann electrostatic Tanimoto coefficient (ET\_pb) and the shape Tanimoto (ST). ET\_pb is determined by comparing the electrostatic potential of the input compound and the query molecule based on an outer dielectric of 80. ST represents the volume overlap of the two molecules. The resulting virtual screening hits were exported as MDL SD-file and analyzed in terms of structural diversity by a Pipeline Pilot script.

**Structural Similarity Analysis of Virtual Screening Hits.** The structural similarity analysis of the virtual screening hits was performed by executing a Pipeline Pilot script that clusters molecules based on Tanimoto similarities between Scitegic's extended connectivity fingerprints (ECFP). Using the ECFP method for calculating structural fingerprints, the environment of every atom of a compound is indexed in order to characterize the molecule. The setting ECFP\_6, which considers all neighbor atoms within a diameter of six bonds for feature calculation of each atom, was utilized.<sup>24</sup> The maximum allowed Tanimoto dissimilarity for assigning compounds to the same structural cluster was set to 0.7.

**hPPAR-LBD Transactivation Assays.** Hepa 1-6 cells were grown in minimum essential medium (MEM) (Gibco) supplemented with 10% FCS and antibiotics (62.5  $\mu$ g/mL penicillin and 100  $\mu$ g/mL streptomycin). A mouse embryo fibroblast (MEF) cell-line was grown in Dulbeccos modified Eagle's media (DMEM) supplemented with 10% calf serum (CS) and antibiotics (62.5  $\mu$ g/mL penicillin and 100  $\mu$ g/mL streptomycin). The cells were seeded in 24-well dishes and transfected at 50–70% confluence.

The Gal4 DNA-binding domain based vector was constructed by inserting the ligand-binding domain of the human PPARs into the pM vector from Invitrogen. The reporter gene was luciferase controlled by the Gal4-responsive UASgal enhancer. As a control vector the bacterial  $\beta$ -galactosidase controlled by the CMV promoter was used (obtained from Clontech). pBSK (Stratagene) was added to obtain optimal plasmid amount for Metafectene transfection.

Hepa 1-6 cells (hPPAR- $\alpha$ ) or MEFs (hPPAR- $\delta$  and - $\gamma$ ) were transfected with Metafectene (Biontix) essentially according to the manufacturer's protocols. In short, for each well in a 24-well plate, a total of 0.35  $\mu$ g of DNA (0.2  $\mu$ g of the Gal4-responsive luciferase reporter 4xUAS-TK-Luc, 0.1  $\mu$ g of a plasmid encoding a fusion between the Gal4 DNA-binding domain, and the human PPAR ligand-binding domain (0.001  $\mu$ g of hPPAR- $\alpha$ -LBD) (additional 0.099  $\mu$ g pBSK (Stratagene) were included with hPPAR- $\alpha$ -LBD), and 0.05  $\mu$ g of the CMV- $\beta$ -galactosidase normalization vector (Clontech) were diluted in 30  $\mu$ L of MEM (hPPAR- $\alpha$ ) or DMEM (hPPAR- $\delta$  and - $\gamma$ ) and mixed with 1  $\mu$ L of Metafectene diluted in 30  $\mu$ L of MEM (hPPAR- $\alpha$ ) or DMEM (hPPAR- $\delta$  and - $\gamma$ ). After 20 min of incubation, the DNA/lipid mixture was added to the cells. Six hours later, the media was changed to MEM (hPPAR- $\alpha$ ) or DMEM (hPPAR- $\delta$  and - $\gamma$ ) supplemented with antibiotics and positive control (30 nM GW7647, 1  $\mu$ M L165041, both from Calbiochem, or 1  $\mu$ M Rosiglitazone, Cayman Chemicals), vehicle, or the compound tested. All compounds were tested in three

concentrations as indicated. The cells were harvested in 100  $\mu$ L of lysis buffer and luciferase and  $\beta$ -galactosidase activities were measured in a LUMIstar Galaxy luminometer (BMG Labtech) according to standard protocols 18 h later.

All experiments were performed in triplicates and measured in duplicates. Luminometer raw data was analyzed in Microsoft Excel spreadsheets. Luciferase activities was normalized for  $\beta$ -galactosidase activity and presented as fold induction relative to vehicle-treated (0.1% DMSO) cells with columns depicting average values  $\pm$  standard deviations of triplicates.

**Competitive Binding Assay.** IC<sub>50</sub> values for respective compounds were determined by competitive binding using time-resolved fluorescence resonance energy transfer (LanthaScreen, Invitrogen) on a Victor2 microplate reader (PerkinElmer). Briefly, a terbium-labeled anti-GST antibody was used to label purified GST-tagged LBD derived from the respective PPAR subtype. Energy transfer from terbium to the tracer, a fluorescent pan PPAR agonist, enabled read-out of each test compound's ability to displace the tracer. RFU values from dose-response curves (triplicate sampling) for test compounds as well as positive controls (GW7647 for PPAR- $\alpha$ , L165041 for PPAR- $\delta$ , and Rosglitazone for PPAR- $\gamma$ ) were then analyzed using GraphPad Prism (GraphPad Software). An unrestrained sigmoidal (one-binding site) dose-response curve was fitted to each data set by linear regression and allowing for determination of IC<sub>50</sub> values.

**Docking of Novel PPAR Ligands.** Docking Studies of PPAR agonists **2**, **5**, **7**, **8**, and **9** were performed within the software Gold 3.1.<sup>41</sup> The default settings of Gold were applied, and GoldScore was selected as the scoring function. For ligand preparation, the software Corina,<sup>42</sup> OpenBabel,<sup>43,44</sup> and Omega were executed. Corina was used to convert the 2D structures of the virtual screening hits into 3D structural data. Subsequently, the protonation states of the compounds at physiological pH were calculated by the molecule file conversion tool OpenBabel. Finally, energy minimization of the 3D structures was performed by the conformer generator Omega. The protein was prepared for docking within the molecular modeling software package Sybyl 7.2.1<sup>45</sup> by removing all ligands and water molecules and by calculating the protonation state of the protein. To improve the accuracy of the binding mode prediction, the GOLD constraint editor was used to add hydrogen bonds and hydrophobic constraints to the docking workflow. These constraints were determined within LigandScout by generating a shared feature pharmacophore model based on agonist-PPAR PDB complexes. The PDB entries 1i7g and 1k7l include crystallographic data of agonist-PPAR- $\alpha$  complexes and therefore formed the basis for a shared feature model for the PPAR- $\alpha$  agonist docking workflow. The shared feature model generated for the PPAR- $\alpha$  agonist docking workflow consisted of three hydrogen bonds formed between the ligand and residues Ser280, Tyr314, and Tyr464 of the protein, as well as three hydrophobic contacts to residues of arm I and II of PPAR- $\alpha$ . To find the best PDB entry for the PPAR- $\alpha$  agonist docking workflow, the resolution of the crystal structures in Å was analyzed. On that account, the protein included in PDB entry 1i7g was selected for the PPAR- $\alpha$  agonist docking workflow. For validation, the crystal structure ligand of this PDB complex was redocked. Because a low rmsd value does not automatically correspond to a docking pose that includes the most important ligand-protein interactions,<sup>46</sup> we did not rely on the rmsd value for validating the docking workflow. Instead of this, we used LigandScout for analyzing and visually investigating the ligand-protein interactions of the docking poses. For PDB entry 1i7g, none of the docking poses was able to reproduce a significant number of the key ligand-protein interactions. However, four out of ten docking poses resulting from the redocking of PDB entry 1k7l were able to form most of the important ligand-protein interactions. The docking pose which represented, except for one hydrophobic contact, all ligand-protein interactions, was ranked fourth by GoldScore. Therefore, the ligand-binding pocket of PDB entry 1k7l was selected for the PPAR- $\alpha$  agonist docking workflow.

The shared feature model for the PPAR- $\gamma$  agonist docking workflow was derived from the agonist-PPAR- $\gamma$  PDB complexes

1fm6, 1fm9, 1i7i, 1k74, 1knu, 1nyx, 1wm0, 2f4b, and 2prg. The model included two hydrophobic interactions located between the ligand and PPAR- $\gamma$  arms II and III, respectively. Again, the best PDB entry in terms of crystal structure resolution was chosen. When the corresponding PDB complex, 2f4b, was validated by redocking the crystal structure ligand, four out of ten docking poses included most of the key ligand-protein interactions. One of these four docking poses was the top-ranked docking solution. Thus, the PPAR- $\gamma$  ligand-binding pocket from PDB complex 2f4b was extracted for PPAR- $\gamma$  agonist docking studies.

Flexible docking of the PPAR antagonist **9** was carried out using the Induced Fit Docking workflow as implemented in the software suite Maestro 8.0.314.<sup>47,48</sup> For the purpose of ligand and protein preparation, LigPrep<sup>49</sup> and the Protein Preparation Wizard of Maestro<sup>48</sup> were executed, respectively. The PDB entry 2awh was selected for the PPAR- $\delta$  antagonist docking workflow because of its high crystal structure resolution and a successful redocking of the crystal structure ligand.

The final docking workflows were used for predicting the putative binding mode of the novel PPAR ligands.

Because the correlation of experimental affinity data and scoring functions is controversially discussed,<sup>50-52</sup> the best docking poses for the novel PPAR ligands were selected by not only taking the docking scores but also the results of the visual investigation of all docking poses into account. In other words, a docking pose that represents key ligand-protein interactions described for PPAR ligands in literature was determined to be more accurate than the highest ranked docking solution, which forms ligand-protein interactions that differ significantly from any binding mode known for PPAR ligands. For example, if the hydrophilic headgroup of a high ranked docking pose for a PPAR agonist was not located next to the active site residues, the docking pose was discarded.

**Acknowledgment.** We thank Dr. Rémy D. Hoffmann, Accelrys SARL Paris, for screening the Derwent World Drug Index 2003 database.

**Supporting Information Available:** hPPAR-LBD transactivation assay results for compounds **1-10**. This material is available free of charge via the Internet at <http://pubs.acs.org>.

## References

- Xu, H. E.; Lambert, M. H.; Montana, V. G.; Parks, D. J.; Blanchard, S. G.; Brown, P. J.; Sternbach, D. D.; Lehmann, J. M.; Wisely, G. B.; Willson, T. M.; Kliewer, S. A.; Milburn, M. V. Molecular recognition of fatty acids by peroxisome proliferator-activated receptors. *Mol. Cell* **1999**, *3*, 397-403.
- Blaschke, F.; Takata, Y.; Caglayan, E.; Law, R. E.; Hsueh, W. A. Obesity, peroxisome proliferator-activated receptor, and atherosclerosis in type 2 diabetes. *Arterioscler. Thromb. Vasc. Biol.* **2006**, *26*, 28-40.
- Cabrero, A.; Llaverias, G.; Roglans, N.; Alegret, M.; Sanchez, R.; Adzet, T.; Laguna, J. C.; Vazquez, M. Uncoupling protein-3 mRNA levels are increased in white adipose tissue and skeletal muscle of bezafibrate-treated rats. *Biochem. Biophys. Res. Commun.* **1999**, *260*, 547-556.
- Rakic, B.; Sagan, S. M.; Noestheden, M.; Belanger, S.; Nan, X.; Evans, C. L.; Xie, X. S.; Pezacki, J. P. Peroxisome proliferator-activated receptor alpha antagonism inhibits hepatitis C virus replication. *Chem. Biol.* **2006**, *13*, 23-30.
- Jarvis, M. C.; Gray, T. J. B.; Palmer, C. N. A. Both PPAR $\gamma$  and PPAR $\delta$  influence sulindac sulfide-mediated p21WAF1/CIP1 upregulation in a human prostate epithelial cell line. *Oncogene* **2005**, *24*, 8211-8215.
- He, T.-C.; Chan, T. A.; Vogelstein, B.; Kinzler, K. W. PPAR $\delta$  is an APC-regulated target of nonsteroidal anti-inflammatory drugs. *Cell* **1999**, *99*, 335-345.
- Gupta, R. A.; Tan, J.; Krause, W. F.; Geraci, M. W.; Willson, T. M.; Dey, S. K.; DuBois, R. N. Prostacyclin-mediated activation of peroxisome proliferator-activated receptor delta in colorectal cancer. *Proc. Natl. Acad. Sci. U.S.A.* **2000**, *97*, 13275-80.
- Burgermeister, E.; Schnoebelen, A.; Flament, A.; Benz, J.; Stihle, M.; Gsell, B.; Rufer, A.; Ruf, A.; Kuhn, B.; Marki, H. P.; Mizrahi, J.; Sebokova, E.; Niesor, E.; Meyer, M. A novel partial agonist of peroxisome proliferator-activated receptor-gamma (PPAR $\gamma$ ) recruits PPAR $\gamma$ -coactivator-1 $\alpha$ , prevents triglyceride ac-

- cumulation, and potentiates insulin signaling in vitro. *Mol. Endocrinol.* **2006**, *20*, 809–30.
- (9) Rieusset, J.; Touri, F.; Michalik, L.; Escher, P.; Desvergne, B.; Niesor, E.; Wahli, W. A new selective peroxisome proliferator-activated receptor gamma antagonist with antiobesity and antidiabetic activity. *Mol. Endocrinol.* **2002**, *16*, 2628–44.
- (10) Willson, T. M.; Brown, P. J.; Sternbach, D. D.; Henke, B. R. The PPARs: from orphan receptors to drug discovery. *J. Med. Chem.* **2000**, *43*, 527–550.
- (11) Xu, H. E.; Lambert, M. H.; Montana, V. G.; Plunket, K. D.; Moore, L. B.; Collins, J. L.; Oplinger, J. A.; Kliewer, S. A.; Gampe, R. T. J.; McKee, D. D.; Moore, J. T.; Willson, T. M. Structural determinants of ligand binding selectivity between the peroxisome proliferator-activated receptors. *Proc. Natl. Acad. Sci. U.S.A.* **2001**, *98*, 13919–13924.
- (12) Ebdrup, S.; Pettersson, I.; Rasmussen, H. B.; Deussen, H. J.; Frost, J. A.; Mortensen, S. B.; Fleckner, J.; Pridal, L.; Nygaard, L.; Sauerberg, P. Synthesis and biological and structural characterization of the dual-acting peroxisome proliferator-activated receptor alpha/gamma agonist ragaglitazar. *J. Med. Chem.* **2003**, *46*, 1306–1317.
- (13) Fyffe, S. A.; Alphey, M. S.; Buetow, L.; Smith, T. K.; Ferguson, M. A.; Sorensen, M. D.; Bjorkling, F.; Hunter, W. N. Recombinant human PPAR-beta/delta ligand-binding domain is locked in an activated conformation by endogenous fatty acids. *J. Mol. Biol.* **2006**, *356*, 1005–1013.
- (14) Xu, H. E.; Lambert, M. H.; Montana, V. G.; Plunket, K. D.; Moore, L. B.; Collins, J. L.; Oplinger, J. A.; Kliewer, S. A.; Gampe, R. T. J.; McKee, D. D.; Moore, J. T.; Willson, T. M. Structural determinants of ligand binding selectivity between the peroxisome proliferator-activated receptors. *Proc. Natl. Acad. Sci. U.S.A.* **2001**, *98*, 13919–13924.
- (15) Xu, H. E.; Stanley, T. B.; Montana, V. G.; Lambert, M. H.; Shearer, B. G.; Cobb, J. E.; McKee, D. D.; Galardi, C. M.; Plunket, K. D.; Nolte, R. T.; Parks, D. J.; Moore, J. T.; Kliewer, S. A.; Willson, T. M.; Stimmel, J. B. Structural basis for antagonist-mediated recruitment of nuclear co-repressors by PPARalpha. *Nature*. **2002**, *415*, 813–817.
- (16) Ye, F.; Zhang, Z. S.; Luo, H. B.; Shen, J. H.; Chen, K. X.; Shen, X.; Jiang, H. L. The dipeptide H-Trp-Glu-OH shows highly antagonistic activity against PPARgamma: bioassay with molecular modeling simulation. *ChemBioChem* **2006**, *7*, 74–82.
- (17) Wolber, G.; Langer, T. LigandScout: 3-D pharmacophores derived from protein-bound ligands and their use as virtual screening filters. *J. Chem. Inf. Model.* **2005**, *45*, 160–169.
- (18) Berman, H. M.; Westbrook, J.; Feng, Z.; Gilliland, G.; Bhat, T. N.; Weissig, H.; Shindyalov, I. N.; Bourne, P. E. The protein data bank. *Nucleic Acids Res.* **2000**, *28*, 235–242.
- (19) Clement, O. O.; Mehl, A. T. HipHop: Pharmacophores based on multiple common-feature alignments. In *Pharmacophore Perception, Development, and Use in Drug Design*; International University Line: La Jolla, CA, 2000; pp 71–84.
- (20) *Catalyst*, version 4.11; Accelrys: San Diego, CA, 2006.
- (21) Markt, P.; Schuster, D.; Kirchmair, J.; Laggner, C.; Langer, T. Pharmacophore modeling and parallel screening for PPAR ligands. *J. Comput.-Aided Mol. Des.* **2007**, *21*, 575–590.
- (22) Muchmore, S. W.; Souers, A. J.; Akritopoulou-Zanze, I. The use of three-dimensional shape and electrostatic similarity searching in the identification of a melanin-concentrating hormone receptor 1 antagonist. *Chem. Biol. Drug Des.* **2006**, *67*, 174–176.
- (23) Kirchmair, J.; Ristic, S.; Eder, K.; Markt, P.; Wolber, G.; Laggner, C.; Langer, T. Fast and efficient in silico 3D screening: Toward maximum computational efficiency of pharmacophore-based and shape-based approaches. *J. Chem. Inf. Model.* **2007**, *47*, 2182–2196.
- (24) Schuster, D.; Laggner, C.; Steindl, T. M.; Hartmann, R. W.; Langer, T. Pharmacophore modeling and in silico screening for new P450 19 (aromatase) inhibitors. *J. Chem. Inf. Model.* **2006**, *46*, 1301–1311.
- (25) Kirchmair, J.; Markt, P.; Distinto, S.; Wolber, G.; Langer, T. Evaluation of the performance of 3D virtual screening protocols: RMSD comparisons, enrichment assessments, and decoy selection: What can we learn from earlier mistakes? *J. Comput.-Aided Mol. Des.* **2007**, *22*, 213–228.
- (26) Szilagi, A.; Skolnick, J. Efficient Prediction of Nucleic Acid Binding Function from Low-Resolution Protein Structures. *J. Mol. Biol.* **2006**, *358*, 922–933.
- (27) Rishton, G. M. Nonleadlikeness and leadlikeness in biochemical screening. *Drug Discovery Today* **2003**, *8*, 86–96.
- (28) Steiner, T. Competition of hydrogen-bond acceptors for the strong carboxyl donor. *Acta Crystallogr., Sect. B: Struct. Sci.* **2001**, *57*, 103–106.
- (29) SciFinder, version 2006; American Chemical Society: Washington, DC, 2006.
- (30) Shen, J.; Shen, X.; Jiang, H.; Luo, X.; Liu, H.; Chen, K.; Shen, J.; Huang, W.; Gui, C.; Chen, Q.; Chen, S.; Sun, T. Preparation of thiazolidine derivatives as PPAR antagonists. Canadian Patent CN 1657529, Feb 20, 2004.
- (31) Yamazaki, Y.; Toma, T.; Nishikawa, M.; Ozawa, H.; Okuda, A.; Araki, T.; Abe, K.; Oda, S. *Preparation ofazole compounds as PPARagonists*. PCT Int. Appl. WO 2005023777, Sep 2, 2004.
- (32) Nieland, T. J. F.; Shaw, J. T.; Jaipuri, F. A.; Maliga, Z.; Duffner, J. L.; Koehler, A. N.; Krieger, M. Influence of HDL-cholesterol-elevating drugs on the in vitro activity of the HDL receptor SR-BI. *J. Lipid Res.* **2007**, *48*, 1832–1845.
- (33) Astarita, G.; Di Giacomo, B.; Gaetani, S.; Oveisi, F.; Compton, T. R.; Rivara, S.; Tarzia, G.; Mor, M.; Piomelli, D. Pharmacological characterization of hydrolysis-resistant analogs of oleoylethanolamide with potent anorexiatic properties. *J. Pharmacol. Exp. Ther.* **2006**, *318*, 563–570.
- (34) *Derwent World Drug Index*, version 2003; Thomson Scientific: London, UK, 2003.
- (35) *ilib:diverse*, version 1.0.2; Inte:Ligand: Maria Enzersdorf, Austria, 2006.
- (36) *Pipeline Pilot*, version 5.0.1.100; Scitegic: San Diego, CA, 2006.
- (37) *MOE*, version 2007.09; CCG: Montreal, 2007.
- (38) *ROCS*, version 2.3.1; Openeye Scientific Software Inc.: Santa Fe, NM, 2007.
- (39) *EON*, version 2.0.1; Openeye Scientific Software Inc.: Santa Fe, NM, 2007.
- (40) *Omega*, version 2.2.1; Openeye Scientific Software Inc.: Santa Fe, NM, 2007.
- (41) *Gold*, version 3.1; CCDC: Cambridge, UK, 2006.
- (42) *CORINA*, version 3.00; Molecular Networks: Erlangen, Germany, 2003.
- (43) Guha, R.; Howard, M. T.; Hutchison, G. R.; Murray-Rust, P.; Rzepa, H.; Steinbeck, C.; Wegner, J. K.; E., W. The Blue Obelisk: Interoperability in Chemical Informatics. *J. Chem. Inf. Model.* **2006**, *46*, 991–998.
- (44) *The Open Babel Package*, version 2.1.0, 2007; <http://openbabel.sourceforge.net/>.
- (45) *Sybyl*, version 7.2.1; Tripos: St. Louis, MO, 2006.
- (46) Kroemer, R. T.; Vulpetti, A.; McDonald, J. J.; Rohrer, D. C.; Trosset, J.-Y.; Giordanetto, F.; Cotesta, S.; McMartin, C.; Kihlen, M.; Stouten, P. F. W. Assessment of docking poses: interactions-based accuracy classification (IBAC) versus crystal structure deviations. *J. Chem. Inf. Comput. Sci.* **2004**, *44*, 871–881.
- (47) *Schrödinger Suite 2007 Induced Fit Docking Protocol: Glide*, version 4.5; Schrödinger, LLC: New York, 2005; Prime, version 1.6; Schrödinger LLC: New York, 2005.
- (48) *Maestro*, version 8.0.314; Schrödinger LLC: New York, 2007.
- (49) *LigPrep*, version 2.1; Schrödinger LLC: New York, 2005.
- (50) Warren, G. L.; Andrews, C. W.; Capelli, A.-M.; Clarke, B.; LaLonde, J.; Lambert, M. H.; Lindvall, M.; Nevins, N.; Semus, S. F.; Senger, S.; Tedesco, G.; Wall, I. D.; Woolven, J. M.; Peishoff, C. E.; Head, M. S. A Critical Assessment of Docking Programs and Scoring Functions. *J. Med. Chem.* **2006**, *49*, 5912–5931.
- (51) Takada, I.; Yu, R. T.; Xu, H. E.; Lambert, M. H.; Montana, V. G.; Kliewer, S. A.; Evans, R. M.; Umehono, K. Alteration of a single amino acid in peroxisome proliferator-activated receptor-alpha (PPAR alpha) generates a PPAR delta phenotype. *Mol. Endocrinol.* **2000**, *14*, 733–740.
- (52) Yanagisawa, H.; Takamura, M.; Yamada, E.; Fujita, S.; Fujiwara, T.; Yachi, M.; Isobe, A.; Hagsawa, Y. Novel oximes having 5-benzyl-2,4-thiazolidinedione as antihyperglycemic agents: synthesis and structure–activity relationship. *Bioorg. Med. Chem. Lett.* **2000**, *10*, 373–375.